THE JOURNAL OF PHYSICAL CHEMISTRY LETTERS
A JOURNAL OF THE AMERICAN CHEMICAL SOCIETY

pubs.acs.org/JPCL

Letter

Molecular Dynamics Studies of Atomistically Determined Fibrillar Assemblies: Comparison of the Rippled β-Sheet, Pleated β-Sheet, and Herringbone Structures

Hyeonju Lee, Moon Young Yang, Jevgenij A. Raskatov, Hyungjun Kim, and William A. Goddard III*

Cite This: *J. Phys. Chem. Lett.* 2024, 15, 4568−4574

Read Online

ACCESS | Metrics & More | Article Recommendations | Supporting Information

ABSTRACT: Pauling and Corey expected that a racemic mixture would result in a rippled β-sheet, however, it has been known from experiments that the racemic mixtures of triphenylalanine lead to a herringbone structure. Because of the theoretical limitations concerning crystal structures such as rippled β-sheet, it is inevitable to understand how the interplay of the amino acids prefers a specific structural motif. In this paper we use molecular dynamics to understand the sequence- and enantiomer-dependent structures by comparisons between rippled β-sheet and pleated β-sheet, solvated and anhydrous rippled β-sheet, and rippled β-sheet and the herringbone structure, based on thermodynamics and structures at the atomic level. The tripeptides select the favored structure that can be stabilized through aromatic or hydrogen bonding interactions between tripeptides. Furthermore, the solubility is determined by the environment of space that is created around the side chains. Our findings provide comprehensive insight into the crystallized fibril motif of the polypeptide.

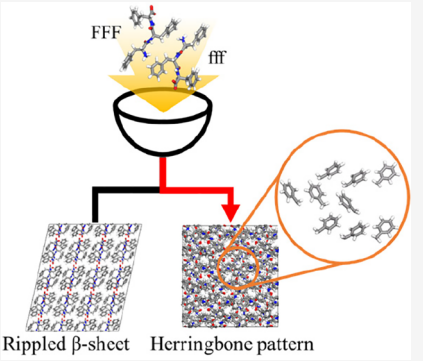

Amyloid-β (Aβ) is an aggregating peptide believed to be the seminal etiological agent of Alzheimer's Disease (AD).[1] The FDA recently approved antibody-based methods to target aggregated Aβ, but their efficacy remains very limited, and treatment is often found to lead to harmful side-effects, such as cerebral bleeding.[2−5] Recently, as one of the various strategies for developing treatments for AD, *Aβ Chiral Inactivation* (Aβ-CI) was proposed that mixing the D-amino acids in equal proportion to the L-amino acids of Aβ 40 and 42 residue assemblies might aggregate as racemic fibrillar assemblies that might suppress formation of neurotoxic oligomeric species.[6−10] This suggested that the blending of D-Aβ might lead to thermodynamic and kinetic effects that favor formation of the rippled β-sheet structure in D,L-Aβ fibrils, preventing formation of the L-fibrils. This motivated our study comparing the stability of the pleated β-sheet (the conventional β-sheet) and the rippled β-sheet structures and how they depend on the chirality.

Between 1951 and 1953, Pauling and Corey conceived the concept of the "pleated β-sheet", known as the conventional β-sheet, and the "rippled β-sheet" predicted from theoretical considerations.[11,12] They predicted that heterochiral/racemic mixtures, where D- and L-peptides are alternately aligned, would form rippled β-sheets, whereas the homochiral/enantiopure form pleated β-sheets. The pleated β-sheet has become a common textbook example, whereas the rippled β-sheet has remained obscure for decades. Extensive research conducted on proteins adopting the pleated β-sheet has led to profound understanding of this motif.[13−16] In contrast, initial experimental evidence for the rippled β-sheet being viable did not emerge until the 1970s.[17−20] In fact, much of the critical momentum for the rippled β-sheet came together over the past decade.[6,10,21−29] The X-ray structural foundation for the rippled β-sheet is only now beginning to emerge,[22,30,31] and the theory foundation for the rippled β-sheet remains extremely limited.

Intriguingly, there are racemic mixtures that do *not* form the rippled β-sheet structure. Since phenylalanine (Phe, F or f) is hydrophobic with a bulky side chain and tends to favor crystallization due to its relative rigidity, the mixtures of (L,L,L)-triphenylalanine (FFF) and (D,D,D)-triphenylalanine (fff) are expected to be the smallest peptides potentially capable of forming a rippled β-sheet.[31] However, crystallization led to a herringbone structure ($[FFF:fff]_n$), composed of repeating rippled β-sheet dimer units (FFF:fff) instead of the rippled β-sheet.[31] To obtain an extended rippled β-sheet layer, it was found that replacing the middle residue in FFF and fff by L- and D-tyrosine (Tyr, Y or y) to form FYF and fyf, respectively, or tryptophan (Trp, W or w) to form FWF and fwf, respectively, increased the solubility of the tripeptides.[22] They succeeded in obtaining periodic antiparallel rippled β-

Received: January 11, 2024
Revised: April 5, 2024
Accepted: April 8, 2024
Published: April 19, 2024

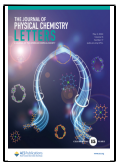

https://doi.org/10.1021/acs.jpclett.4c00101
J. Phys. Chem. Lett. 2024, 15, 4568−4574

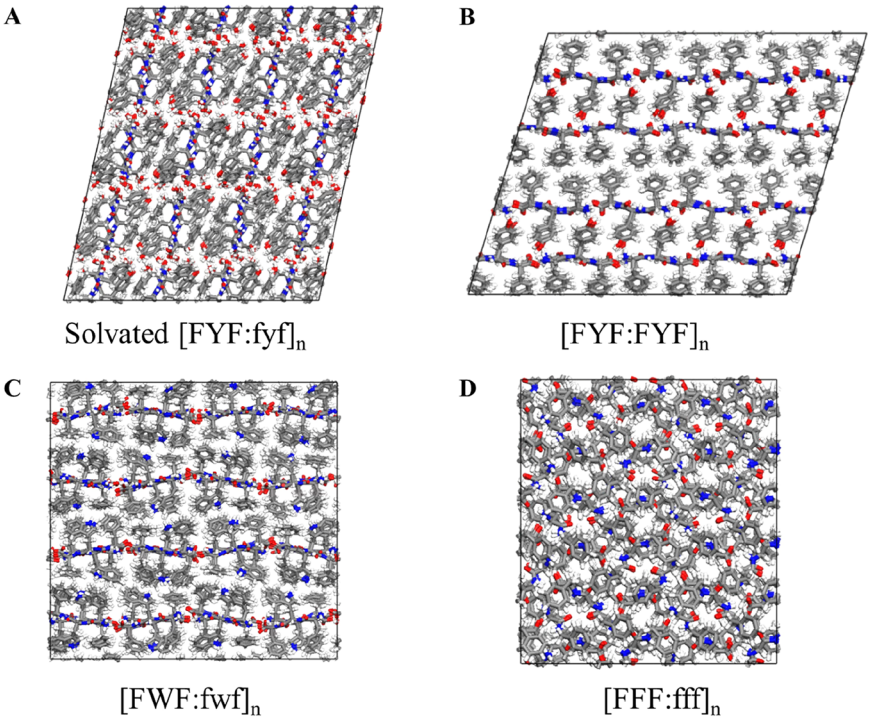

Figure 1. Snapshots from molecular dynamics (MD) simulations at 300 K of (A) rippled β-sheet solvated $[FYF:fyf]_n$, (B) pleated β-sheet $[FYF:FYF]_n$, (C) rippled β-sheet $[FWF:fwf]_n$, and (D) herringbone structure $[FFF:fff]_n$ equilibrium states. The initial structures were obtained by X-ray crystallography.

sheets (solvated $[FYF:fyf]_n$ and $[FWF:fwf]_n$) which they compared with the parallel pleated β-sheet ($[FYF:FYF]_n$) and herringbone structure ($[FFF:fff]_n$).[22,31]

In this paper, we investigate the following questions using molecular dynamics (MD) simulations of solvated $[FYF:fyf]_n$, $[FYF:FYF]_n$, $[FWF:fwf]_n$, and $[FFF:fff]_n$, starting with X-ray crystal structures where available, to establish both the thermodynamics and structures of rippled β-sheet, pleated β-sheet, and herringbone structures at the atomic level:[22,31]

(1) Comparing the rippled β-sheet of solvated $[FYF:fyf]_n$ and the pleated β-sheet structures of $[FYF:FYF]_n$, why does FYF form a crystallized rippled β-sheet when mixed with fyf, instead of self-sorting from each other and aggregating into homochiral $[FYF:FYF]_n$ forms?

(2) Comparing the solvated rippled β-sheet of solvated $[FYF:fyf]_n$ and the anhydrous rippled β-sheet of $[FWF:fwf]_n$, why is $[FYF:fyf]_n$ soluble in water but $[FWF:fwf]_n$ is not, forming a racemic rippled β-sheet structure? What role does water play in stabilizing the peptides in solvated $[FYF:fyf]_n$?

(3) Comparing the rippled β-sheet of solvated $[FYF:fyf]_n$ and the herringbone structure of $[FFF:fff]_n$, why does $[FFF:fff]_n$ form the herringbone structure instead of a rippled β-sheet structure?

Our studies aim to address these questions, revealing how the interaction between the mirror images of tripeptides can induce crystallization with unique properties to specific types of crystal structure. Our findings indicate that the stability of the crystallized fibril structures is achieved by forming a configuration that prevents steric hindrance while allowing strong binding between side chains. The environment generated by this arrangement of side chains allows the fibril to be solvated by water, stabilizing the racemic fibril. We hope to utilize these insights to provide valuable guidelines for designing potential therapeutic agents for neurodegenerative diseases including AD. We also examine the feasibility of using solvated agents to provide valuable clues.

METHODS

We started with the unit cells of solvated $[FYF:fyf]_n$, $[FYF:FYF]_n$, $[FWF:fwf]_n$, and $[FFF:fff]_n$ from X-ray crystallography (Figure S1).[22,31,32] We then created supercells containing 72 to 128 tripeptides (4536 to 8192 atoms) for use in MD studies. The number of tripeptides, water molecules, and atoms in these supercells is summarized in Table S1. Additionally, based on these supercells, we generated $[fyf:fyf]_n$, anhydrous $[FYF:fyf]_n$, and $[FFF:fff]_n$ with rippled β-sheet and $[FYF:fyf]_n$ with herringbone structure.

We used the GROMACS MD software[33] with the CHARMM36 force field (FF)[34] to describe the interatomic interactions of the tripeptide and the TIP3P[35] FF to describe the water molecule.

The temperature and pressure were controlled by the modified Berendsen[36] thermostats and Berendsen[37] barostats with coupling constants of 1 and 2 ps at 300 K and 1 bar, respectively. We set the time step as 2 fs and employed the Particle-Mesh Ewald method[38] for long-range electrostatic interactions. The cutoff distances were chosen as 1.5 nm for both van der Waals and electrostatic interactions. The linear constraints solver (LINCS) algorithm[39] was used to impose constraints on bonds with H atoms.

We ran isothermal-isobaric ensemble (NPT) MD 10 times for 2 ns each using force restraints that gradually reduced the force applied to the side chain by factors of 2 until it reached 0 from 1000 over 12 ns. Similarly, we reduced the force applied to the backbone until it corresponded to 0 over 8 ns (Figure S2). After this, we ran NPT MD without restraints for 20 ns

https://doi.org/10.1021/acs.jpclett.4c00101
J. Phys. Chem. Lett. 2024, 15, 4568−4574

followed by canonical ensemble (NVT) MD for 20 ns using the equilibrium lattice parameters determined from the NPT run. Finally, we ran NVT MD for an additional 10 ns to produce the results. The final structures of the four different systems are shown in Figure 1.

To validate how well the systems obtained from crystallography kept their cell sizes throughout MD simulation, we compare the lattice parameters obtained from X-ray crystallography and MD supercell simulations in Table S2. They remain similar in size with a difference less than 4.39%. Furthermore, the root-mean-square deviation (RMSD) of the backbone relative to the backbone from crystallography is less than 0.1 nm during the last 10 ns (Figure S3).

Experimental results demonstrate that enantiopure FYF ($[FYF:FYF]_n$) forms the pleated β-sheet motif, while FYF and fyf adopt the rippled β-sheet motif while incorporating water molecules (solvated $[FYF:fyf]_n$).[22] Thus, it is not thermodynamically favorable for FYF and fyf to self-sort into chiral entities when heterochiral molecules are mixed. Using the difference in the total energy of the bulk structure and single tripeptides, defined as the cohesive energy density (CED), we predict the thermodynamic stability. We analyzed the CED for solvated $[FYF:fyf]_n$, $[FYF:FYF]_n$, artificially generated $[fyf:fyf]_n$, and anhydrous $[FYF:fyf]_n$ to form both pleated β-sheet and rippled β-sheet structures (Table 1). These results indicate

Table 1. Cohesive Energy Density (CED) of Solvated $[FYF:fyf]_n$, $[FYF:FYF]_n$, Artificially Generated $[fyf:fyf]_n$, and Anhydrous $[FYF:fyf]_n$

	CED (kJ/mol/nm^3)
Solvated $[FYF:fyf]_n$	−1046.11
$[FYF:FYF]_n$	−864.29
$[fyf:fyf]_n$	−852.68
Anhydrous $[FYF:fyf]_n$	−671.55

that solvated $[FYF:fyf]_n$ with the rippled β-sheet motif is substantially more stable than $[FYF:FYF]_n$ and $[fyf:fyf]_n$ with the pleated β-sheet motif, explaining why FYF and fyf do not self-sort.

The increased stability of rippled β-sheet-solvated $[FYF:fyf]_n$ compared to pleated β-sheet $[FYF:FYF]_n$ can be understood from a structural perspective. Figure 2A shows that the solvated $[FYF:fyf]_n$ backbones form hydrogen bonding (HB) interactions, leading to the formation of rippled dimers, and that they form salt bonds with adjacent rippled dimers. Figure 2E shows that the backbones of the pleated β-sheet $[FYF:FYF]_n$ form salt bridge and HB interactions similarly, but unlike solvated $[FYF:fyf]_n$, the homochiral system forms HB interactions between the backbone and phenol of the side chain in Figure 2F. Examining the interactions between side chains, solvated $[FYF:fyf]_n$ shows aromatic interactions between the phenol groups of the middle residues (Tyr) that are positioned perpendicular to the salt bridge and facing each other (Figure 2B). The FYF and fyf adopt either a parallel displacement (Figure 2C) or a Y-shaped aromatic interaction (Figure 2D) between the benzene rings. Similarly, we find that $[FYF:FYF]_n$, predominantly demonstrates a $\pi-\pi$ stacking interaction between phenols or benzene rings (Figure 2G) and parallel displacement between benzenes (Figure 2H).

We analyze the average number of HB interactions (N_{HB}) normalized by the number of tripeptides ($N_{peptide}$) within each system. The N_{HB} of solvated $[FYF:fyf]_n$ is higher than that of

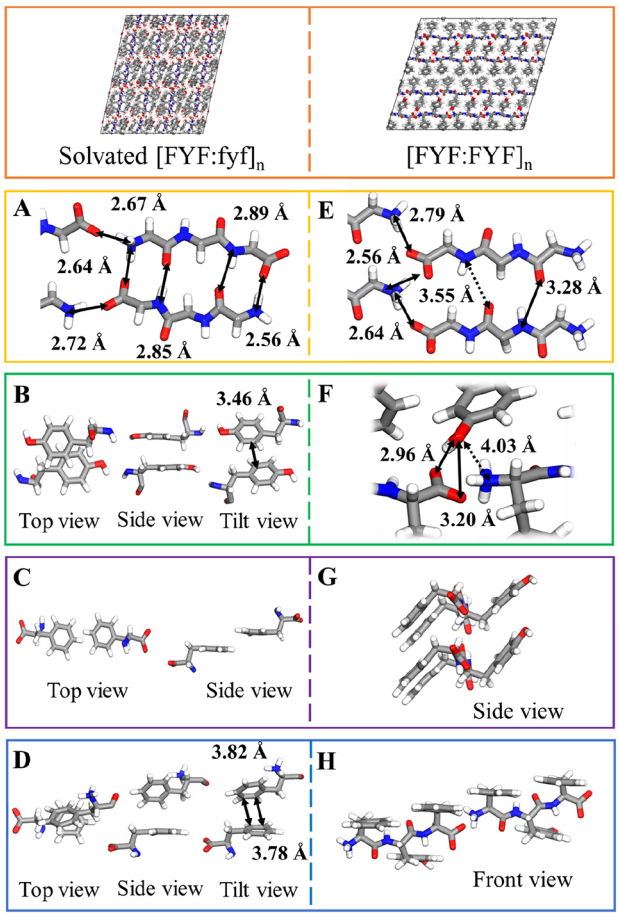

Figure 2. Hydrogen bonding (HB) or aromatic interaction in solvated $[FYF:fyf]_n$ and $[FYF:FYF]_n$ in terms of various perspectives between backbones or side chains. (A, E) Multiple HB interactions between backbones. Solid arrows represent the distance between atoms that form HBs, while dashed arrows indicate the distance between atoms that are too far apart to engage in HB interactions. (B) Aromatic interaction between two phenols. (C) Parallel displacement aromatic interaction between benzene rings. (D) Y-shaped aromatic interaction between benzene rings. (F) Multiple HB interactions between the phenol of the side chain and the C termini of the backbone. (G) $\pi-\pi$ stacking aromatic interaction between benzene rings or phenols. (H) Parallel displacement aromatic interaction between benzene rings. Gray, blue, red, and white denote C, N, O, and H, respectively.

$[FYF:FYF]_n$, but excluding interactions with water molecules, the N_{HB} of $[FYF:FYF]_n$ is higher. These findings are consistent with the CED result, demonstrating that solvated $[FYF:fyf]_n$ is more stable than $[FYF:FYF]_n$ and $[fyf:fyf]_n$, while anhydrous $[FYF:fyf]_n$ is the least stable.

Additionally, through a comparison of non-bond interaction energy (E_{nb}), combining Lennard-Jones and Coulomb interaction energy and normalized by $N_{peptide}$, between backbones or side chains, we first note that the contribution of aromatic interactions between side chains outweighs that of interactions between backbones (Figure S6). The E_{nb} values between backbones or side chains in the solvated $[FYF:fyf]_n$ are notably stronger compared to those in $[FYF:FYF]_n$. Our calculations demonstrate that the interactions between side chains in solvated $[FYF:fyf]_n$ are more favorable than those in $[FYF:FYF]_n$. The stronger interactions in solvated $[FYF:fyf]_n$ result in its backbone and side chain having diffusion coefficients (D) 1.85 and 1.77 times slower than those for

https://doi.org/10.1021/acs.jpclett.4c00101
J. Phys. Chem. Lett. 2024, 15, 4568−4574

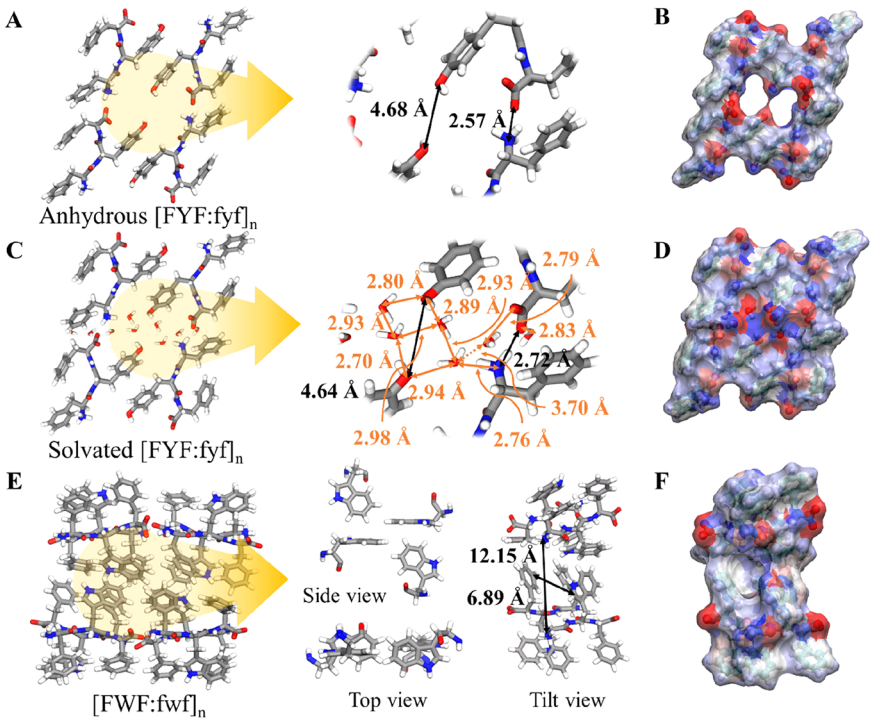

Figure 3. (A) The hydrogen bonding (HB) interactions in the vacant region between phenols or C and N termini of tripeptide in artificially generated anhydrous $[FYF:fyf]_n$. (B) The HB interactions among 6 water molecules and C and N termini of tripeptides in solvated $[FYF:fyf]_n$. (C) The HB interactions of the 4 Trp side chains from the top and side view and the empty space between the Trp and Phe side chains from the tilt view in $[FWF:fwf]_n$. Gray, blue, red, and white denote C, N, O, and H, respectively. (D−F) Electric potentials of tripeptides of (D) anhydrous $[FYF:fyf]_n$, (E) solvated $[FYF:fyf]_n$, and (F) $[FWF:fwf]_n$, respectively. The color changes from red to white to blue as the charge changes from negative to zero to positive.

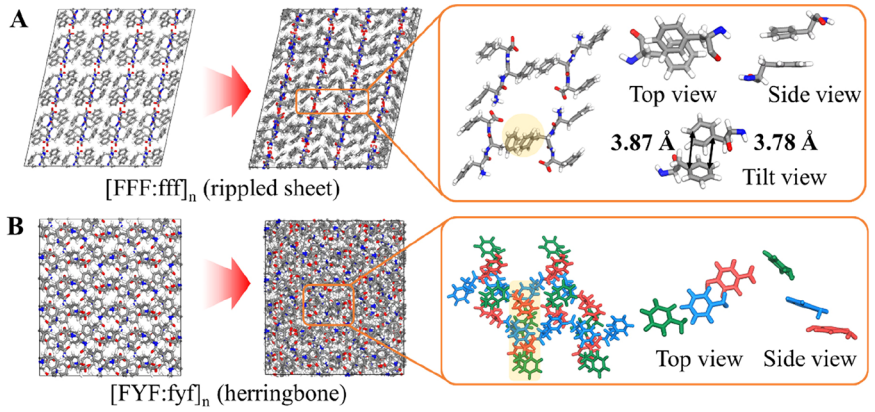

Figure 4. (A) The initial and equilibrium structure of the artificially created $[FFF:fff]_n$ with rippled β-sheet form by replacing the OH end of the middle Tyr side chain from the anhydrous $[FYF:fyf]_n$ with rippled β-sheet. The substituted benzene ring replacing the phenol interacts in Y-shaped aromatic interactions with a neighboring benzene ring. (B) The initial and equilibrium structure of the artificially generated anhydrous $[FYF:fyf]_n$ with herringbone structure by adding OH at the end of the middle Phe side chain for the $[FFF:fff]_n$ with herringbone structure. The substituted phenol and benzene rings interact in parallel aromatic interactions. Gray, blue, red, and white denote C, N, O, and H, respectively.

$[FYF:FYF]_n$ based on the two-phase thermodynamics (2PT) analysis[40] (Table S3).

The solvated $[FYF:fyf]_n$ is significantly more stable thermodynamically than artificially created anhydrous $[FYF:fyf]_n$ (Table 1), indicating the crucial role of water molecules in stabilizing the system. Next, we investigate solvated $[FYF:fyf]_n$ and $[FWF:fwf]_n$, both of which select the rippled β-sheet, as well as artificially created anhydrous $[FYF:fyf]_n$ to understand the role of water in the stability. In anhydrous $[FYF:fyf]_n$ (Figure 3A) and solvated $[FYF:fyf]_n$ (Figure 3C), the two phenol groups that are parallel to the salt bridge pack to form an empty space between them because they interact at distances of 4.68 and 4.64 Å, respectively. However, in the solvated $[FYF:fyf]_n$ this empty space is filled by 6 water molecules that participate in HB interaction with the OH of the phenol groups, with the N and C termini of the peptide, or with each other, forming a HB network that contributes considerably to stabilizing solvated $[FYF:fyf]_n$. All water molecules in solvated $[FYF:fyf]_n$ are in this empty space (Figure S7).

In contrast, $[FWF:fwf]_n$ containing bulkier Trp in place of Tyr, does not lead to empty regions between the Trp side

https://doi.org/10.1021/acs.jpclett.4c00101
J. Phys. Chem. Lett. 2024, 15, 4568−4574

chains because the rippled β-sheet structure is stabilized by interactions between Trp's in a T-shape arrangement (Figure 3E top and side views). Despite there being spaces for water incorporation between the benzene rings (Figure 3E tilt view), it remains anhydrous because benzene rings surround this empty space, leading to a hydrophobic environment with much lower polarity than that of anhydrous $[FYF:fyf]_n$ (Figure 3B and F). Despite having the same rippled β-sheet structure, a hydrophilic environment surrounding the empty space is required for dissolution in water. Thus, the packing of hydrophilic side chains is pivotal in shaping these empty spaces.

Indeed, even though both are racemic mixtures, solvated $[FYF:fyf]_n$ forms a rippled β-sheet, while $[FFF:fff]_n$ is anhydrous, displaying a fibril structure with a herringbone structure. A key difference between Phe-Phe-Phe and Phe-Tyr-Phe lies in the hydroxyl (OH) group located at the end of the middle residue of Tyr.[22] We generated $[FFF:fff]_n$ with rippled β-sheet by substituting OH with H in the Tyr of the anhydrous $[FYF:fyf]_n$ with rippled β-sheet and then equilibrating in the same manner as in the other systems. Figure 4A shows that the equilibrium state of the $[FFF:fff]_n$ with rippled β-sheet cannot sustain its structure. In the solvated $[FYF:fyf]_n$ with rippled β-sheet, the phenols interact with water molecules in a direction parallel to the salt bridge, but in the $[FFF:fff]_n$ with rippled β-sheet, as the phenol is replaced by benzene rings, it prefers stabilizing through $\pi-\pi$ interactions with an adjacent benzene ring, as shown in Figure 4A, rather than those positioned distantly and diagonally. Indeed, the CED of the $[FFF:fff]_n$ with rippled β-sheet is substantially higher than that of the herringbone structure (Table S5). Consequently, despite being a racemic mixture, $[FFF:fff]_n$ stabilizes the system by selecting the herringbone structure instead of the rippled β-sheet.

On the other hand, we also generated the anhydrous $[FYF:fyf]_n$ with herringbone structure by substituting H with OH as Tyr in the $[FFF:fff]_n$ with herringbone structure and compared the CED (Table S5). In contrast to the rippled β-sheet $[FFF:fff]_n$, the herringbone structure anhydrous $[FYF:fyf]_n$ is relatively stable due to the aromatic interaction among the benzene rings and phenols of FYF:fyf rippled dimer in a parallel displacement arrangement (Figure 4B), thereby preventing steric hindrance as in the herringbone structure $[FFF:fff]_n$ (Figure S8). However, the rippled β-sheet of anhydrous $[FYF:fyf]_n$ is more stable than the herringbone structure. This is because the aromatic interaction between phenols is much stronger within the rippled β-sheet than the aromatic interaction in the form of parallel displacement between phenol and benzenes in a herringbone structure. From our findings, we discovered that the arrangement of tripeptides is determined by the strong interaction between side chains.

In this study, we investigated the influence of the chemical nature of side chain on the racemic tripeptide fibril motif with the aim of providing the basis for understanding the fibril motif found crystallographically for these tripeptides that we hope will be useful for designing and developing AD therapeutic agents utilizing Aβ-CI. We examined various tripeptide fibrils using conducted MD simulations to analyze the equilibrium structures to achieve comprehensive insights into the thermodynamic basis for structural stability. Our investigations revealed that the stability of the racemic structure is attained by adopting an arrangement of side chains that prevents steric hindrance while promoting strong binding interactions between the side chains. The specific arrangement of side chains in solvated $[FYF:fyf]_n$ generates an environment that allows water to solvate the fibril, dramatically enhancing stability. New insights include the following:

(1) By comparing the rippled β-sheet structure of solvated $[FYF:fyf]_n$ with pleated β-sheet, $[FYF:FYF]_n$, and $[fyf:fyf]_n$, we discovered that the rippled β-sheet is thermodynamically more stable with water. We attribute this stability to the strong HB interactions with water molecules and aromatic interactions. Consequently, the mixture of FYF and fyf prefers the rippled β-sheet motif of the racemic dimer.

(2) By comparing the solvated rippled β-sheet $[FYF:fyf]_n$ with anhydrous rippled β-sheet $[FYF:fyf]_n$ and $[FWF:fwf]_n$, we found that in solvated $[FYF:fyf]_n$, water molecules dissolve into the empty spaces formed by a pair of phenols, stabilizing the system by forming a HB network with solvated water molecules, neighboring phenols, and the N and C termini of the tripeptides. The solubility of water is enhanced and determined by the environment of the empty space.

(3) By comparing the rippled β-sheet and the herringbone structure for anhydrous $[FYF:fyf]_n$, we discovered that the stability of racemic Phe-Tyr-Phe with the herringbone structure is relatively low, while the rippled β-sheet motif provides stronger aromatic interaction between side chains. In contrast, comparing the rippled β-sheet and herringbone structure of $[FFF:fff]_n$, we found that replacing the phenols of Tyr with benzene increases the distance between benzenes, preventing aromatic interactions. This leads to destruction of the rippled β-sheet structure, forming instead the herringbone structure that allows interaction with adjacent benzenes.

This computational study highlights the importance of interactions between polypeptides in stabilizing crystallized fibrils, which we hope provides comprehensive understanding of racemic polypeptide fibrils that may extend beyond tripeptides, to design potential therapeutic agents of neurodegenerative disease including AD through Aβ-CI.

■ ASSOCIATED CONTENT

Supporting Information

The Supporting Information is available free of charge at https://pubs.acs.org/doi/10.1021/acs.jpclett.4c00101.

Figure S1 shows the initial unit cell obtained from X-ray crystallography. Figure S2 shows the change of the force applied to the systems during NPT MD simulation. Figure S3 shows the change in RMSD of systems obtained from X-ray crystallography. Figure S4 shows representative MD snapshots of anhydrous $[FYF:fyf]_n$ and $[fyf:fyf]_n$. Figure S5 shows the optimized FYF, fyf, FFF, and fff configurations with potential energy. Figure S6 shows the E_{nb} between BB-BB and SC-SC in the solvated $[FYF:fyf]_n$ and $[FYF:FYF]_n$. Figure S7 shows the probability of finding water molecules and the projected snapshot of solvated $[FYF:fyf]_n$. Figure S8 shows the 8 tripeptides of $[FFF:fff]_n$ with several HBs between backbones and parallel displacement aromatic interaction among the benzene rings. Table S1 summarizes the number of peptides, water molecules, and atoms for all systems. Table S2 compares the lattice parameters of the supercell obtained from X-ray

https://doi.org/10.1021/acs.jpclett.4c00101
J. Phys. Chem. Lett. 2024, 15, 4568−4574

crystallography and the equilibrium lattice parameters from MD simulation. Table S3 compares the diffusion coefficients of BB and SC in solvated $[FYF:fyf]_n$ and $[FYF:FYF]_n$. Table S4 lists the number of HB interactions in solvated $[FYF:fyf]_n$ and $[FYF:FYF]_n$. Table S5 shows the CED values for $[FFF:fff]_n$ and anhydrous $[FYF:fyf]_n$ with a herringbone structure and rippled β-sheet structure. (PDF)

AUTHOR INFORMATION

Corresponding Author

William A. Goddard III − *Materials and Process Simulation Center, California Institute of Technology, Pasadena, California 91125, United States*; Email: wag@caltech.edu

Authors

Hyeonju Lee − *Department of Chemistry, Korea Advanced Institute of Science and Technology (KAIST), Daejeon 34141, Republic of Korea; Materials and Process Simulation Center, California Institute of Technology, Pasadena, California 91125, United States*

Moon Young Yang − *Materials and Process Simulation Center, California Institute of Technology, Pasadena, California 91125, United States*

Jevgenij A. Raskatov − *UC Santa Cruz Department of Chemistry and Biochemistry, UCSC, Santa Cruz, California 95064, United States*

Hyungjun Kim − *Department of Chemistry, Korea Advanced Institute of Science and Technology (KAIST), Daejeon 34141, Republic of Korea; Materials and Process Simulation Center, California Institute of Technology, Pasadena, California 91125, United States*

Complete contact information is available at: https://pubs.acs.org/10.1021/acs.jpclett.4c00101

Notes

The authors declare no competing financial interest.

ACKNOWLEDGMENTS

WAG thanks the US NSF (CBET 2311117) for support. JAR thanks the NIH for the award R01AG074954 and the Seaver Institute for a generous gift. Prof. Harry B. Gray is gratefully acknowledged for helpful discussions.

REFERENCES

(1) Selkoe, D. J.; Hardy, J. The Amyloid Hypothesis of Alzheimer's Disease at 25 Years. *EMBO Mol. Med.* **2016**, *8*, 595−608.

(2) Abbott, A. Could Drugs Prevent Alzheimer's? These Trials Aim to Find Out. *Nat.* **2022**, *603*, 216−219.

(3) Grossmann, K. Direct Oral Anticoagulants (DOACs) for Therapeutic Targeting of Thrombin, a Key Mediator of Cerebrovascular and Neuronal Dysfunction in Alzheimer's Disease. *Biomedicines* **2022**, *10*, 1890−1923.

(4) Mullard, A. Alzheimer's Drug Approval Could Affect Other Diseases. *Nat.* **2021**, *595*, 162−163.

(5) Jeremic, D.; Jiménez-Díaz, L.; Navarro-López, J. D. Past, Present and Future of Therapeutic Strategies against Amyloid-β Peptides in Alzheimer's Disease: A Systematic Review. *Ageing Res. Rev.* **2021**, *72*, 101496−101531.

(6) Dutta, S.; Foley, A. R.; Warner, C. J. A.; Zhang, X.; Rolandi, M.; Abrams, B.; Raskatov, J. A. Suppression of Oligomer Formation and Formation of Non-Toxic Fibrils upon Addition of Mirror-Image Aβ42 to the Natural l-Enantiomer. *Angew. Chem., Int. Ed.* **2017**, *56*, 11506−11510.

(7) Raskatov, J. A. Chiral Inactivation: An Old Phenomenon with a New Twist. *Chem. − Eur. J.* **2017**, *23*, 16920−16923.

(8) Sonzini, S.; Stanyon, H. F.; Scherman, O. A. Decreasing Amyloid Toxicity through an Increased Rate of Aggregation. *Phys. Chem. Chem. Phys.* **2017**, *19*, 1458−1465.

(9) Bieschke, J.; Herbst, M.; Wiglenda, T.; Friedrich, R. P.; Boeddrich, A.; Schiele, F.; Kleckers, D.; Amo, J. M. L. d.; Gürning, B.; Wang, Q.; Schmidt, M. R.; Lurz, R.; Anwyl, R.; Schnoegl, S.; Fändrich, M.; Frank, R. F.; Reif, B.; Günther, S.; Walsh, D. M.; Wanker, E. E. Small-molecule Conversion of Toxic Oligomers to Nontoxic β-Sheet-Rich Amyloid Fibrils. *Nat. Chem. Biol.* **2012**, *8*, 93−101.

(10) Raskatov, J. A.; Foley, A. R.; Louis, J. M.; Yau, W. M.; Tycko, R. Constraints on the Structure of Fibrils Formed by a Racemic Mixture of Amyloid-β Peptides from Solid-State NMR, Electron Microscopy, and Theory. *J. Am. Chem. Soc.* **2021**, *143*, 13299−13313.

(11) Pauling, L.; Corey, R. B. The Pleated Sheet, a New Layer Configuration of Polypeptide Chains. *Proc. Natl. Acad. Sci. U. S. A.* **1951**, *37*, 251−256.

(12) Pauling, L.; Corey, R. B. Two Rippled-sheet Configurations of Polypeptide Chains, and a Note about the Pleated Sheets. *Proc. Natl. Acad. Sci. U. S. A.* **1953**, *39*, 253−256.

(13) Ihsan, N.S. M. N.; Sani, S.F. A.; Looi, L. M.; Cheah, P. L.; Chiew, S. F.; Pathmanathan, D.; Bradley, D. A. A review: Exploring the Metabolic and Structural Characterisation of Beta Pleated Amyloid Fibril in Human Tissue using Raman Spectrometry and SAXS. *Prog. Biophys. Mol. Biol.* **2023**, *182*, 59−74.

(14) Glenner, G. G.; Eanes, E. D.; Bladen, H. A.; Linke, R. P.; Termine, J. D. β-Pleated Sheet Fibrils a Comparison of Native Amyloid with Synthetic Protein Fibrils. *J. Histochem. Cytochem.* **1974**, *22*, 1141−1158.

(15) Chothia, C; Levitt, M; Richardson, D Structure of proteins: Packing of A-helices and Pleated Sheets. *Proc. Natl. Acad. Sci. U. S. A.* **1977**, *74*, 4130−4134.

(16) Lokeyl, R. S.; Iverson, B. L. Synthetic Molecules that Fold into a Pleated Secondary Structure in Solution. *Nat.* **1995**, *375*, 303−305.

(17) Lotz, B. Crystal Structure of Polyglycine I. *J. Mol. Biol.* **1974**, *87*, 169−180.

(18) Colonna-Cesari, F.; Premilat, S.; Lotz, B. Structure of Polyglycine I: A Comparison of the Antiparallel Pleated and Antiparallel Rippled Sheets. *J. Mol. Biol.* **1974**, *87*, 181−191.

(19) Moore, W. H.; Krimm, S. Vibrational Analysis of Peptides, Polypeptides, and Proteins. I. Polyglycine I. *Biopolymers* **1976**, *15*, 2439−2464.

(20) Lotz, B. Rippled Sheets: The Early Polyglycine Days and Recent Developments in Nylons. *ChemBioChem.* **2022**, *23*, e202100658−202100665.

(21) Raskatov, J. A. A DFT Study of Structure and Stability of Pleated and Rippled Cross-Beta Sheets with Hydrophobic Sidechains. *Biopolymers* **2021**, *112*, e23391−233396.

(22) Hazari, A.; Sawaya, M. R.; Vlahakis, N.; Johnstone, T. C.; Boyer, D.; Rodriguez, J.; Eisenberg, D.; Raskatov, J. A. The Rippled β-sheet Layer Configuration—a Novel Supramolecular Architecture Based on Predictions by Pauling and Corey. *Chem. Sci.* **2022**, *13*, 8947−8952.

(23) Raskatov, J. A.; Schneider, J. P.; Nilsson, B. L. Defining the Landscape of the Pauling-Corey Rippled Sheet: An Orphaned Motif Finding New Homes. *Acc. Chem. Res.* **2021**, *54*, 2488−2501.

(24) Raskatov, J. A. Conformational Selection as the Driving Force of Amyloid β Chiral Inactivation. *ChemBioChem.* **2020**, *21*, 2945−2949.

(25) Nagy-Smith, K.; Beltramo, P. J.; Moore, E.; Tycko, R.; Furst, E. M.; Schneider, J. P. Molecular, Local, and Network-Level Basis for the Enhanced Stiffness of Hydrogel Networks Formed from Coassembled Racemic Peptides: Predictions from Pauling and Corey. *ACS Cent. Sci.* **2017**, *3*, 586−597.

(26) Nagy, K. J.; Giano, M. C.; Jin, A.; Pochan, D. J.; Schneider, J. P. Enhanced Mechanical Rigidity of Hydrogels Formed from Enantio-

meric Peptide Assemblies. *J. Am. Chem. Soc.* **2011**, *133*, 14975−14977.
(27) Urban, J. M.; Ho, J.; Piester, G.; Fu, R.; Nilsson, B. L. Rippled β-Sheet Formation by an Amyloid-β Fragment Indicates Expanded Scope of Sequence Space for Enantiomeric β-Sheet Peptide Coassembly. *Molecules* **2019**, *24*, 1983−1995.
(28) Swanekamp, R. J.; Welch, J. J.; Nilsson, B. L. Proteolytic Stability of Amphipathic Peptide Hydrogels Composed of Self-assembled Pleated β-Sheet or Coassembled Rippled β-Sheet Fibrils. *Chem. Commun.* **2014**, *50*, 10133−10136.
(29) Swanekamp, R. J.; Dimaio, J. T. M.; Bowerman, C. J.; Nilsson, B. L. Coassembly of Enantiomeric Amphipathic Peptides into Amyloid-inspired Rippled β-sheet Fibrils. *J. Am. Chem. Soc.* **2012**, *134*, 5556−5559.
(30) Lotz, B. Original Crystal Structures of Even-Even Polyamides Made of Pleated and Rippled Sheets. *Macromolecules* **2021**, *54*, 551−564.
(31) Kuhn, A. J.; Ehlke, B.; Johnstone, T. C.; Oliver, S. R. J.; Raskatov, J. A. A Crystal-Structural Study of Pauling−Corey Rippled Sheets. *Chem. Sci.* **2022**, *13*, 671−680.
(32) Raskatov, J. A.; Foley, A. R.; Louis, J. M.; Yau, W. M.; Tycko, R. Constraints on the Structure of Fibrils Formed by a Racemic Mixture of Amyloid-β Peptides from Solid-State NMR, Electron Microscopy, and Theory. *J. Am. Chem. Soc.* **2021**, *143*, 13299−13313.
(33) Van Der Spoel, D.; Lindahl, E.; Hess, B.; Groenhof, G.; Mark, A. E.; Berendsen, H. J. C. GROMACS: Fast, Flexible, and Free. *J. Comput. Chem.* **2005**, *26*, 1701−1718.
(34) Huang, J.; Mackerell, A. D. CHARMM36 All-Atom Additive Protein Force Field: Validation Based on Comparison to NMR data. *J. Comput. Chem.* **2013**, *34*, 2135−2145.
(35) Mark, P.; Nilsson, L. Structure and Dynamics of the TIP3P, SPC, and SPC/E Water Models at 298 K. *J. Phys. Chem. A* **2001**, *105*, 9954−9960.
(36) Berendsen, H. J. C. Transport Properties Computed by Linear Response through Weak Coupling to a Bath. Springer: Netherlands, 1991; pp 139−155.
(37) Berendsen, H. J. C.; Postma, J. P. M.; Van Gunsteren, W. F.; Dinola, A.; Haak, J. R. Molecular Dynamics with Coupling to an External Bath. *J. Chem. Phys.* **1984**, *81*, 3684−3690.
(38) Darden, T.; York, D.; Pedersen, L. Particle Mesh Ewald: An N·log(N) Method for Ewald Sums in Large Systems. *J. Chem. Phys.* **1993**, *98*, 10089−10092.
(39) Hess, B.; Bekker, H.; Berendsen, H. J. C.; Fraaije, J. G. E. M. LINCS: A Linear Constraint Solver for molecular simulations. *J. Comput. Chem.* **1997**, *18*, 1463−1472.
(40) Lin, S. T.; Maiti, P. K.; Goddard, W. A. Two-Phase Thermodynamic Model for Efficient and Accurate Absolute Entropy of Water from Molecular Dynamics Simulations. *J. Phys. Chem. B* **2010**, *114*, 8191−8198.

https://doi.org/10.1021/acs.jpclett.4c00101
J. Phys. Chem. Lett. 2024, 15, 4568−4574